

# An investigation of the small slope approximation for scattering from rough surfaces. Part II. Numerical studies

Shira Lynn Broschat

*School of Electrical Engineering and Computer Science, Washington State University, Pullman, Washington 99164-2752*

Eric I. Thorsos

*Applied Physics Laboratory, College of Ocean and Fishery Sciences, University of Washington, Seattle, Washington 98105*

(Received 3 May 1996; revised 1 November 1996; accepted 1 December 1996)

The small slope approximation (SSA) of Voronovich [Sov. Phys. JETP **62**, 65–70 (1985)] is a promising method for modeling wave scattering from rough surfaces. The SSA  $T$ -matrix series, which can be interpreted as an expansion in a generalized surface slope, satisfies the appropriate reciprocity condition at each order and reduces to the standard perturbation series for small surface roughness. When the SSA  $T$  matrix is found to second order in generalized slope, it reduces to that of the Kirchhoff approximation as the frequency is increased. In an earlier paper [E. I. Thorsos and S. L. Broschat, *J. Acoust. Soc. Am.* **97**, 2082–2093 (1995)] the derivation of the SSA for surfaces subject to the Dirichlet boundary condition was examined in detail. In this paper the accuracy of the SSA for the Dirichlet problem is investigated through comparison with exact results. Expressions for the first three terms of the SSA incoherent bistatic scattering cross-section series are presented, followed by numerical results for one-dimensional surfaces with Gaussian statistics and a Gaussian roughness spectrum. Surfaces with rms slope angles up to  $45^\circ$  are considered. It is found that, for the numerous cases studied, the SSA results agree well with the exact results over a broad range of scattering angles. When the lowest-order results are inaccurate, successive addition of each higher-order term generally yields improvement. The range of scattering angles over which the SSA results are accurate depends on both the rms slope angle and the surface correlation length, as well as on the angle of incidence. A simple rule of thumb, however, is that for an incident angle of  $45^\circ$ , the highest-order SSA scattering cross section examined here is accurate to within  $\pm 1$  dB from backscatter to a forward grazing angle of  $5^\circ$  for rms slope angles less than about  $30^\circ$ . When the surface roughness is such that perturbation theory is accurate, the SSA is accurate over the full range of scattering angles for small to moderate slopes. © 1997 Acoustical Society of America. [S0001-4966(97)06405-9]

PACS numbers: 43.30.Hw, 43.20.Fn [JHM]

## INTRODUCTION

In the past two decades much research has been done on wave scattering from rough surfaces. A major objective has been to devise an analytic model for bistatic scattering that is accurate when the small perturbation method and Kirchhoff approximation apply but, in addition, is accurate in regions where they do not apply. One of the more promising of the new methods is the small slope approximation (SSA), which was introduced by Voronovich in the mid-1980s (1985, 1986).

In Part I of this two-part series (Thorsos and Broschat, 1995), we presented a derivation of the SSA for the Dirichlet problem and discussed in detail the assumptions made. The SSA takes the form of a systematic expansion that can be interpreted as a series in a generalized surface slope (henceforth, referred to simply as slope), as discussed later. The series is manifestly reciprocal at each order, and reduction to standard perturbation theory is inherent in the derivation. The first three terms in the small slope series  $T$  matrix— $T_0$ ,  $T_1$ , and  $T_2$ —are derived in Part I.

Several numerical studies of the small slope approxima-

tion for rough surface scattering are available in the literature. Berman (1991) has compared Monte Carlo SSA results for bistatic scattering with exact results for both the Dirichlet and fluid–solid boundaries for one-dimensional (1-D) surfaces satisfying a Pierson–Moskowitz power-law spectrum (Dirichlet boundary) or a modified power-law spectrum (fluid–solid boundary). Broschat (1993) has compared formally averaged (theoretical) results for the reflection coefficient with exact results for a Pierson–Moskowitz power-law spectrum. These initial comparisons with exact calculations give encouraging support for the accuracy of the SSA. In addition, Yang and Broschat (1992, 1994) have presented results for 2-D surface, bistatic scattering for the Dirichlet problem for a Gaussian spectrum as well as 1-D surface results for acoustic scattering from a fluid–elastic-solid interface for both Gaussian and modified power-law spectra.

In this paper we investigate the validity of the SSA for scalar-wave scattering from 1-D, randomly rough surfaces satisfying the Dirichlet boundary condition and having Gaussian statistics and a Gaussian roughness spectrum. We consider the first three terms of the SSA series for the bistatic scattering cross section,  $\sigma$ , and compare SSA results for the

formally averaged bistatic scattering strength ( $= 10 \log_{10} \sigma$ ) with exact Monte Carlo integral equation results. As discussed in Sec. I, these terms in the SSA series are second, third, and fourth order in slope, respectively.

Surfaces characterized by a Gaussian spectrum are single-scale surfaces, and the surface correlation length determines this scale. The correlation length can be varied to yield, at one extreme, surfaces with only small-scale roughness and, at the other, surfaces with only large-scale roughness. Thus, use of the Gaussian spectrum over the full range of correlation lengths and bistatic scattering angles provides a useful test of the SSA for varying length scales of roughness. A detailed study of low grazing angle scattering with application to power-law-type spectra will be presented in the future. Preliminary results have been reported for the lowest-order SSA cross section using a Pierson–Moskowitz power-law spectrum, and these are encouraging (Broschat and Thorsos, 1995).

In this numerical study we consider several aspects of the SSA for an incident angle of  $45^\circ$ , unless otherwise noted. First we examine the SSA for surfaces with a modest rms slope angle of  $10^\circ$ . The SSA is generally very accurate for these cases, although as the surface correlation length is increased, scattering is underpredicted at low grazing angles of scatter in the back direction and the SSA cross section becomes a little high at forward grazing angles less than about  $5^\circ$ . The underprediction at low grazing angles depends on the surface roughness parameters used and may extend up to  $10^\circ$ ,  $20^\circ$ , or even  $30^\circ$ .

Next we compare the SSA with perturbation theory for surfaces with small roughness. The lowest-order term in the series for the SSA scattering cross section is generally accurate when lowest-order perturbation theory is accurate. There is an important difference in the manner in which the two approximations become inaccurate. For moderate slopes, the lowest-order SSA remains accurate near the specular direction for all  $kh$  (where  $k$  is the wave number and  $h$  is the rms surface height). However, for  $kh > 1$  the lowest-order perturbation result becomes inaccurate over the entire angular range. Addition of both third- and fourth-order terms in the SSA cross-section series yields accurate results in and significantly beyond the region where higher-order perturbation theory is accurate (Thorsos and Jackson, 1989). Only beyond the perturbation theory regime do the results become low in the back direction and high at forward grazing angles less than  $5^\circ$  as the correlation length is increased.

Comparison of the SSA and perturbation theory is followed by comparison of the small slope and Kirchhoff approximations. In the Kirchhoff regime, the SSA and Kirchhoff approximation results agree well over a broad range of scattering angles. For scattering angles in the backward direction the lowest-order SSA prediction is lower than the Kirchhoff prediction when the Kirchhoff approximation is accurate. [For the Gaussian spectrum, the Kirchhoff approximation becomes inaccurate at grazing angles less than about twice the rms slope angle. See Thorsos (1988) for further discussion.] Successive addition of third- and fourth-order terms improves the result, but the SSA prediction is still slightly low. In the forward direction the lowest-order SSA is

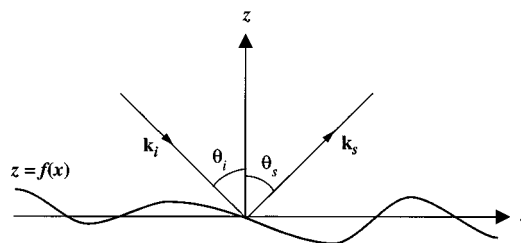


FIG. 1. Scattering geometry.

very accurate at all but the lowest grazing angles ( $< 5^\circ$ ) for moderate surface slopes, unlike the Kirchhoff approximation whose results are typically high over a considerably larger grazing angle region.

As noted in Part I, the sum of the first two terms in the SSA  $T$ -matrix series reduces to the Kirchhoff approximation  $T$  matrix as the frequency is increased. When the corresponding terms in the SSA cross-section series are retained, reduction to the Kirchhoff cross section occurs as the frequency is increased. We find, however, that this reduction, first to the Kirchhoff approximation result and then to the geometrical optics result, occurs very slowly with increasing frequency for forward-scattering angles near grazing. Comparison with exact calculations shows that the SSA is accurate in this region, except at angles less than about  $5^\circ$  grazing, for rms surface heights at least up to one-and-a-half wavelengths.

In addition to the studies above, we investigate the accuracy of the fourth-order SSA for  $kh$  fixed and  $kl$  increasing (decreasing slope) and for  $kl$  fixed and  $kh$  increasing (increasing slope), where  $l$  is the surface correlation length. In general, we find that the fourth-order SSA and exact results agree well over a broad range of scattering angles for rms slope angles less than about  $30^\circ$ . In particular, we find that the results become low in the back direction as  $kl$  is increased; however, for increasing  $kh$  they remain remarkably accurate as the surface slope approaches 1, that is, as the surface slope angle approaches  $45^\circ$ , except at scattering angles near grazing where they become high.

For most of the cases examined the angle of incidence is  $45^\circ$ ; however, for two cases we also consider incident angles of  $0^\circ$  and  $80^\circ$ . The first case uses a moderate correlation length, and the fourth-order SSA results are excellent for both incident angles. The second case uses a longer correlation length, and the range of angles over which the fourth-order SSA is accurate becomes smaller as the incident angle is increased.

In Sec. I the terminology used for the SSA slope orders is described, and expressions for the first three terms of the SSA bistatic scattering cross-section series are given. Numerical results are presented in Sec. II.

## I. BISTATIC SCATTERING CROSS SECTIONS

Since our numerical studies are for 1-D surfaces (the 2-D scattering problem), we restrict our derivation to this case; however, extension to 2-D surfaces is straightforward. Our scattering geometry is shown in Fig. 1 with the rough surface denoted by  $z = f(x)$ . The incident field is a scalar

plane wave  $\exp[i\mathbf{k}_i \cdot \mathbf{r}]$  with  $\mathbf{r}=(x,z)$  and  $\mathbf{k}_i=(k_{ix},k_{iz})=(k_{ix},-\kappa_{iz})$ , where  $\kappa_{iz}=[k^2-k_{ix}^2]^{1/2}>0$  and  $k=\omega/c$  is the radiation wave number. The small slope series for the  $T$  matrix is written as  $T=T_0+T_1+T_2+\dots$ . The first two terms of this expansion are given by

$$T_0(k_{sx},k_{ix})=-\frac{2\kappa_{iz}}{\nu_z}\frac{1}{2\pi}\int dx \exp[i\mathbf{v}\cdot\mathbf{r}]|_{z=f(x)}, \quad (1)$$

$$T_1(k_{sx},k_{ix})=\frac{i\kappa_{iz}}{\nu_z}\frac{1}{2\pi}\int dx \exp[i\mathbf{v}\cdot\mathbf{r}]|_{z=f(x)} \\ \times \int dK_1 \exp[iK_1x]F(K_1) \\ \times [k\beta_{1+i}+k\beta_{s-1}-\nu_z], \quad (2)$$

where  $\mathbf{v}=\mathbf{k}_i-\mathbf{k}_s=(\nu_x,-\nu_z)$  so that  $\nu_x=k_{ix}-k_{sx}$  and  $\nu_z=\kappa_{iz}+k_{sz}$ ,  $k\beta_{1+i}=[k^2-(K_1+k_{ix})^2]^{1/2}$  with  $\text{Im}[\beta_{1+i}]>0$ ,  $k\beta_{s-1}=[k^2-(k_{sx}-K_1)^2]^{1/2}$  with  $\text{Im}[\beta_{s-1}]>0$ , and  $F(K)$  is the Fourier transform of  $f(x)$ . Equations (1) and (2) as well as the expression for the third term of the series,  $T_2$ , are derived in Part I. In general, the  $T_n$  term in the  $T$ -matrix series includes  $n$  factors of  $F(K)$ ; in addition, the surface profile  $f(x)$  enters into each term via the factor  $\exp[i(\nu_x x - \nu_z f(x))]$ . As discussed by Voronovich (1985) and in Part I, it can be shown that  $T_0$  is first order in slope,  $T_1$  is second order in slope, and so on. Actually, when we refer to a term as  $n$ th order in slope, we mean  $n$ th order in generalized slope. The term generalized slope is used because, as described in Part I, the integrand of the  $x$  integral in  $T_n$  ( $n>0$ ) can be expressed in a coordinate space series as a product of  $\exp[i\mathbf{v}\cdot\mathbf{r}]$  and a series beginning with the term  $[f'(x)]^{n+1}$  followed by terms in higher powers of  $f'(x)$  as well as by terms involving higher derivatives of  $f(x)$ . For  $n=0$  the coordinate space series begins at  $[f'(x)]^0$  and includes all contributions of order  $f'(x), f''(x), f'''(x), \dots$ . For simplicity, we refer to  $T_n$  as order  $n+1$  in slope. The entire dependence of  $T_n$  on  $k_{sx}$  occurs in the factor  $\exp[i\mathbf{v}\cdot\mathbf{r}]$  in this coordinate space series.

In terms of the  $T$  matrix, the bistatic scattering cross section for scattering from 1-D surfaces is given by (see Appendix A in Berman, 1991, and Appendix B in Thorsos and Jackson, 1989)

$$\sigma\delta(k_{ix}-k'_{ix})=\frac{k_{sz}^2}{k}-[\langle T(k_{sx},k_{ix})T(k_{sx},k'_{ix})^* \rangle \\ -\langle T(k_{sx},k_{ix}) \rangle \langle T(k_{sx},k'_{ix})^* \rangle], \quad (3)$$

where the angle brackets denote an ensemble average, and the asterisk denotes the complex conjugate. The right-hand side of (3) is proportional to  $\delta(k_{ix}-k'_{ix})$  which is a result of the assumed translational invariance of the surface statistics. Using the  $T$ -matrix series,  $T=T_0+T_1+T_2+\dots$ , in (3) then gives the scattering cross-section series,  $\sigma=\sigma_{00}+\sigma_{01}+\sigma_{11}+\dots$ , where

$$\sigma_{00}\delta(k_{ix}-k'_{ix})=\frac{k_{sz}^2}{k}[\langle T_0(k_{sx},k_{ix})T_0(k_{sx},k'_{ix})^* \rangle \\ -\langle T_0(k_{sx},k_{ix}) \rangle \langle T_0(k_{sx},k'_{ix})^* \rangle], \quad (4)$$

$$\sigma_{01}\delta(k_{ix}-k'_{ix})=\frac{k_{sz}^2}{k}2 \text{Re}[\langle T_0(k_{sx},k_{ix})T_1(k_{sx},k'_{ix})^* \rangle \\ -\langle T_0(k_{sx},k_{ix}) \rangle \langle T_1(k_{sx},k'_{ix})^* \rangle], \quad (5)$$

$$\sigma_{11}\delta(k_{ix}-k'_{ix})=\frac{k_{sz}^2}{k}[\langle T_1(k_{sx},k_{ix})T_1(k_{sx},k'_{ix})^* \rangle \\ -\langle T_1(k_{sx},k_{ix}) \rangle \langle T_1(k_{sx},k'_{ix})^* \rangle]. \quad (6)$$

Since  $T_0$  is first order in slope, it follows that  $\sigma_{00}$  is second order in slope. Similarly,  $\sigma_{01}$  and  $\sigma_{11}$  are third and fourth order in slope, respectively. Thus we write the second-, third-, and fourth-order cross sections as

$$\sigma^{(2)}=\sigma_{00}, \quad (7)$$

$$\sigma^{(3)}=\sigma^{(2)}+\sigma_{01}, \quad (8)$$

$$\sigma^{(4)}=\sigma^{(3)}+\sigma_{11}. \quad (9)$$

Note that (9) does not give the complete fourth-order cross section since it is missing the  $\sigma_{02}$  term associated with  $T_0$  and  $T_2$ ; this omission will be discussed later. For simplicity, in this paper we will refer to (9) as the fourth-order cross section.

Evaluation of the formal averages in (4)–(6) is carried out in a way similar to that used for perturbation theory (e.g., Appendix B in Thorsos and Jackson, 1989). However, the moment evaluations are more complicated because, in addition to the factors of  $F(K)$ , the random variable  $f(x)$  in the argument of the exponential function  $\exp[i\mathbf{v}\cdot\mathbf{r}]|_{z=f(x)}$  must be considered. The first moments of  $T_0$  and  $T_1$  are

$$\langle T_0(k_{sx},k_{ix}) \rangle=-\frac{2\kappa_{iz}}{\nu_z}\frac{1}{2\pi}\int dx \exp[i\nu_x x] \\ \times \langle \exp[-i\nu_z f(x)] \rangle \\ =-\exp[-\chi^2/2]\delta(k_{sx}-k_{ix}), \quad (10)$$

$$\langle T_1(k_{sx},k_{ix}) \rangle=\frac{i\kappa_{iz}}{\nu_z}\frac{1}{(2\pi)^2}\int dx \exp[i\nu_x x] \\ \times \int dK_1 \exp[iK_1x][k\beta_{1+i}+k\beta_{s-1} \\ -\nu_z]\int dx' \exp[-iK_1x'] \\ \times \langle \exp[-i\nu_z f(x)]f(x') \rangle \\ =\kappa_{iz} \exp[-\chi^2/2]\delta(k_{sx}-k_{ix}) \\ \times \int dK_1 W(K_1)g(K_1), \quad (11)$$

where

$$\chi=\nu_z h,$$

$$g(K_1)=k\beta_{1+i}+k\beta_{s-1}-\nu_z$$

[note that  $g(K_1)$  can be complex], and  $W(K_1)$  is the surface roughness spectrum given by

$$W(K_1) = \frac{1}{2\pi} \int dx \exp[-iK_1x] \langle f(x_0)f(x+x_0) \rangle.$$

To obtain (11),  $F(K)$  in (2) is expressed as the Fourier transform of  $f(x)$ , giving a moment of the form  $\langle \exp[i\alpha_1 X_1] X_2 \rangle$ , where  $X_1$  and  $X_2$  are zero-mean Gaussian random variables. This moment is found by use of the identity

$$\langle e^{i\alpha_1 X_1} X_2 \rangle = -i \left. \frac{\partial \langle e^{i\alpha_1 X_1} e^{i\alpha_2 X_2} \rangle}{\partial \alpha_2} \right|_{\alpha_2=0}. \quad (12)$$

The partial derivative in (12) is readily evaluated using (Parzen, 1962)

$$\langle e^{i\alpha_1 X_1} e^{i\alpha_2 X_2} \rangle = \exp[-(1/2)(\alpha_1^2 \langle X_1^2 \rangle + 2\alpha_1 \alpha_2 \langle X_1 X_2 \rangle + \alpha_2^2 \langle X_2^2 \rangle)]. \quad (13)$$

The second moments are obtained similarly as described shortly. When evaluating the right-hand sides of (4)–(6), the result for each contains a factor of  $\delta(k_{ix} - k'_{ix})$ , which then cancels out to give the cross section terms. The integral in (1) is identical to that of the Kirchhoff approximation (Ishimaru, 1978). Thus, the result of performing the formal averages in (4) differs from that of the Kirchhoff approximation by a coefficient only, and the second-order SSA cross section is given by

$$\sigma^{(2)} = \frac{2k_{sz}^2 \kappa_{iz}^2}{\pi k \nu_z^2} \exp[-\chi^2] \int dx \exp[i\nu_x x] B_C(x), \quad (14)$$

where

$$B_C(x) = \exp[\chi^2 C(x)] - 1,$$

where  $C(x)$  is the surface correlation function normalized so that  $C(0) = 1$  and is given by

$$C(x)h^2 = \langle f(x_0)f(x+x_0) \rangle = \int dK W(K) \exp[iKx].$$

The relationship between the second-order SSA and Kirchhoff approximation cross sections is given by

$$\sigma^{(2)} = \sigma_{KA} / g^2, \quad (15)$$

where

$$g = \frac{\kappa_{iz} \nu_z - k_{ix} \nu_x}{2k_{sz} \kappa_{iz}}. \quad (16)$$

In the specular direction  $g=1$ , and (14) reduces to the Kirchhoff approximation cross section.

The terms  $\langle T_0 T_1^* \rangle$  and  $\langle T_1 T_1^* \rangle$  in (5) and (6) contain ensemble averages of the type  $\langle e^{i\alpha_1 X_1} e^{i\alpha_2 X_2} X_3 \rangle$  and  $\langle e^{i\alpha_1 X_1} e^{i\alpha_2 X_2} X_3 X_4 \rangle$  where  $X_1$  through  $X_4$  are zero-mean Gaussian random variables. The latter average can be found using

$$\langle e^{i\alpha_1 X_1} e^{i\alpha_2 X_2} X_3 X_4 \rangle = - \left. \frac{\partial^2 \langle e^{i\alpha_1 X_1} e^{i\alpha_2 X_2} e^{i\alpha_3 X_3} e^{i\alpha_4 X_4} \rangle}{\partial \alpha_3 \partial \alpha_4} \right|_{\alpha_3 = \alpha_4 = 0} \quad (17)$$

and the former average using a similar relationship. The partial derivative is readily evaluated using (Parzen, 1962)

$$\begin{aligned} & \langle e^{i\alpha_1 X_1} e^{i\alpha_2 X_2} e^{i\alpha_3 X_3} e^{i\alpha_4 X_4} \rangle \\ & = \exp \left[ - \left( \frac{1}{2} \right) \sum_j \sum_k \alpha_j \alpha_k K_{jk} \right], \end{aligned} \quad (18)$$

where  $K_{jk} = \langle X_j X_k \rangle$ . The final results after some lengthy but straightforward manipulations are given by

$$\begin{aligned} \sigma_{01}(k_{sx}, k_{ix}) & = \frac{2k_{sz}^2 \kappa_{iz}^2}{\pi k \nu_z} \exp[-\chi^2] \\ & \times \text{Re} \left\{ -J^* \int dx \exp[i\nu_x x] B_C(x) \right. \\ & + \int dx I(x) \int dK \exp[iKx] W(K) \\ & \left. \times g^*(K) \right\}, \end{aligned} \quad (19)$$

$$\begin{aligned} \sigma_{11}(k_{sx}, k_{ix}) & = \frac{k_{sz}^2 \kappa_{iz}^2}{2\pi k} \exp[-\chi^2] \\ & \times \left\{ |J|^2 \int dx \exp[i\nu_x x] B_C(x) \right. \\ & + \int dx I(x) \int dK \exp[iKx] W(K) \\ & \times \left\{ \frac{1}{\nu_z^2} |g(K)|^2 - 2 \text{Re}[Jg^*(K)] + g(K) \right. \\ & \left. \left. \times \int dK' \exp[iK'x] W(K') g^*(K') \right\} \right\}, \end{aligned} \quad (20)$$

where

$$I(x) = \exp[i\nu_x x] \exp[\chi^2 C(x)],$$

$$J = \int dK W(K) g(K).$$

Since  $\mathbf{v}$  and  $g(K)$  are both reciprocal, it follows that  $\sigma^{(2)}$ ,  $\sigma_{01}$ , and  $\sigma_{11}$  given by (14), (19), and (20), respectively, all satisfy the reciprocity condition, that is, exchanging  $k_{ix}$  and  $k_{sx}$  with  $-k_{sx}$  and  $-k_{ix}$  results in identical expressions for the cross-section terms. For the angle convention of Fig. 1 the reciprocity condition implies that the cross-section terms are unchanged when  $\theta_i$  and  $\theta_s$  are replaced by  $-\theta_s$  and  $-\theta_i$ . In addition, because of the assumed translational invariance of the surface statistics, moments remain the same when  $f(x)$  is replaced by  $f(-x)$  for each surface in the surface ensemble. It follows that the cross section terms are unchanged when  $\theta_i$  and  $\theta_s$  are replaced by  $-\theta_i$  and  $-\theta_s$ . This combined with the reciprocity condition implies that the cross-section terms do not change when  $\theta_i$  and  $\theta_s$  are replaced by  $\theta_s$  and  $\theta_i$ .

As discussed in Part I (Sec. II) and earlier by Voronovich (1985),  $T_0 + T_1$  reduces to the Kirchhoff approximation  $T$  matrix for large  $k$ . It is straightforward to show the corresponding result for the cross section, that is,  $\sigma^{(4)}$  given by (9) reduces to  $\sigma_{KA}$ , the Kirchhoff approximation cross sec-

tion, for large  $k$ . Thus, in the high-frequency limit as  $k \rightarrow \infty$ ,  $\sigma^{(4)} \rightarrow \sigma_{\text{GO}}$ , the geometrical optics result.

As mentioned earlier in this section, the fourth-order SSA cross section given by (9) is missing the  $\sigma_{02}$  term and, thus, does not contain all possible fourth-order components. This is not consistent with the second- and third-order expressions given by (7) and (8) since they contain all second- and third-order components, respectively. There are several reasons for including  $\sigma_{11}$  and not  $\sigma_{02}$  in (9). As stated in the previous paragraph,  $\sigma^{(4)}$  given by (9) reduces to the Kirchhoff approximation cross section for large  $k$ . This is strong motivation for including  $\sigma_{11}$ . Excluding the  $\sigma_{02}$  term is motivated by the need to balance numerical accuracy and numerical complexity. From (14), (19), and (20), it can be seen that evaluating  $\sigma_{00}$  involves a single integral, while  $\sigma_{01}$  and  $\sigma_{11}$  involve double integrals. Evaluation of the  $\sigma_{02}$  term, not presented here, involves triple integrals. Thus, inclusion of  $\sigma_{02}$  would generally be considered less practical for most applications. Since  $\sigma_{02}$  and  $\sigma_{11}$  are of the same order of slope, they may in fact be of comparable size. However, comparisons with integral equation results show  $\sigma^{(4)}$ , without  $\sigma_{02}$ , to be an improvement over  $\sigma^{(3)}$ . This improvement is sufficient justification for keeping only part of the fourth-order slope contribution to the SSA cross section series.

In standard perturbation theory (PT) a cross-section series in even powers of  $kh$  is obtained. The lowest-order term is denoted  $\sigma_{\text{PT}}^{11}$  or PT(2) and is of order  $(kh)^2$ . [The notation follows that of Thorsos and Jackson (1989) with the subscript PT added to distinguish between perturbation theory and the SSA. The superscript 11 indicates the absolute square of the first-order scattered field.] The next order in the perturbation cross-section series is  $\sigma_{\text{PT}}^{22} + \sigma_{\text{PT}}^{13}$ , where  $\sigma_{\text{PT}}^{13}$  is the contribution from the product of the first- and third-order scattered fields, or equivalently, from the product of the first- and third-order  $T$  matrices. Both  $\sigma_{\text{PT}}^{22}$  and  $\sigma_{\text{PT}}^{13}$  are of order  $(kh)^4$ . For the SSA, as discussed in Part I, the small height expansion of  $T_{\text{SSA}} = T_0 + \dots + T_n$  agrees exactly with standard perturbation theory to order  $(kh)^{n+1}$ . This implies that when  $\sigma^{(2)}$  is expanded in powers of  $kh$ , the lowest-order term is exactly  $\sigma_{\text{PT}}^{11}$ , and additional terms are of higher even powers in  $kh$ . Among these terms are reciprocal approximations to  $\sigma_{\text{PT}}^{22}$  and  $\sigma_{\text{PT}}^{13}$ . When  $\sigma^{(3)}$  is expanded in a perturbation series, these approximations are improved. Finally, in the perturbation expansion of  $\sigma^{(4)}$ , both  $\sigma_{\text{PT}}^{11}$  and  $\sigma_{\text{PT}}^{22}$  are obtained exactly. To obtain  $\sigma_{\text{PT}}^{13}$  exactly, it would be necessary to extend the  $T_{\text{SSA}}$  series through  $T_2$  in order to include  $\sigma_{02}$  in  $\sigma^{(4)}$ . The perturbation expansion of  $\sigma^{(4)}$  would then yield the standard perturbation theory result to order  $(kh)^4$ .

## II. NUMERICAL RESULTS

In this section, the accuracy of the second-, third-, and fourth-order SSA bistatic scattering cross sections— $\sigma^{(2)}$ ,  $\sigma^{(3)}$ , and  $\sigma^{(4)}$ —is examined by comparison with Monte Carlo integral equation calculations (Thorsos, 1988). Numerical results are presented for the scattering strength ( $= 10 \log_{10} \sigma$ ) and are restricted to scalar wave scattering from 1-D Dirichlet surfaces satisfying the Gaussian roughness spectrum as given by

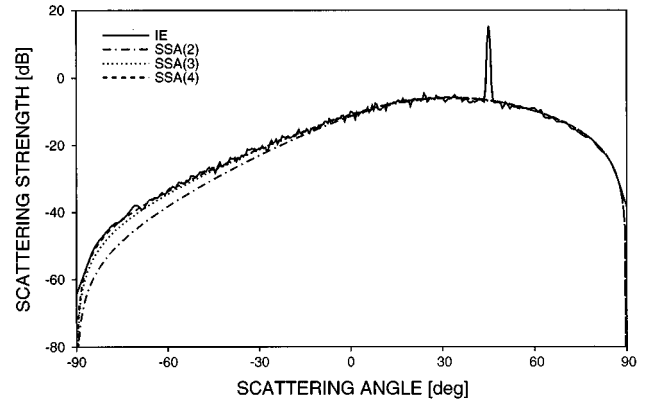


FIG. 2. Comparison of the second-order [SSA(2)], third-order [SSA(3)], and fourth-order [SSA(4)] small slope approximation and Monte Carlo integral equation (IE) scattering strengths ( $= 10 \log_{10} \sigma$ ) for a modest rms surface slope angle. Here  $kh=0.5$ ,  $kl=4.0$ , where  $k$  is the wave number,  $h$  is the rms surface height, and  $l$  is the correlation length, the rms slope angle  $\gamma$  is  $10^\circ$ , and the incident angle  $\theta_i$  is  $45^\circ$ .

$$W(K) = \frac{h^2 l}{(2\sqrt{\pi})} e^{-K^2 l^2 / 4},$$

where  $h$  is the rms surface height and  $l$  is the surface correlation length. For each example we calculate the scattering strength over the complete  $180^\circ$  range of scattering angles for a particular incident angle. When the SSA results agree with exact results to within 1 dB, we consider them to be accurate. However, we limit our investigation to scattering strengths greater than  $-80$  dB.

### A. Accuracy of the SSA for modest surface slopes

We begin by examining two cases with rms surface slope angles of  $10^\circ$ . Figure 2 shows the SSA and exact results when the surface roughness parameters  $kh$  and  $kl$  are 0.5 and 4.0, respectively, the incident angle  $\theta_i$  is  $45^\circ$ , the rms slope  $s$  is 0.177 ( $s = \sqrt{2}h/l$  for Gaussian surfaces), and the rms slope angle  $\gamma$  is  $\tan^{-1} s = 10^\circ$ . The peak in the specular direction of the integral equation result is due to the coherent component of the total cross section and represents specular reflection, which has not been included in the approximate methods. The specular peak can be subtracted out easily, but will be included for most of the cases presented as a qualitative indication of the size of the coherent component. Fluctuations in the integral equation results are due to the finite number of surface realizations used in the ensemble average. Here, 50 realizations have been used. As more surface realizations are added, the fluctuations decrease in magnitude; in the limit of an infinite number of realizations, the curve would be smooth. For details on the integral equation technique, see Thorsos (1988). From Fig. 2 we see that the second-order SSA [SSA(2)] is accurate in the forward direction ( $0^\circ < \theta_s \leq 90^\circ$ ), but it is not accurate in the back direction ( $-90^\circ \leq \theta_s < 0^\circ$ ). The third-order result shows marked improvement, and the fourth-order SSA [SSA(4)] is accurate everywhere.

In Fig. 3  $kh$  and  $kl$  have both been increased by a factor of three to 1.5 and 12.0, respectively, yielding a smoother surface. The coherent component at  $\theta_s = 45^\circ$  is reduced to nearly the incoherent level because of the greater surface height, and the scattering level in the back direction is re-

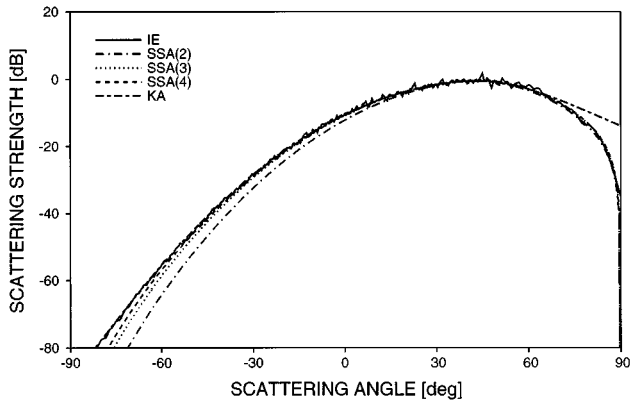


FIG. 3. Comparison of the SSA(2), SSA(3), SSA(4), Kirchhoff approximation (KA), and IE scattering strengths. The rms height and correlation length of Fig. 2 have been increased threefold to  $kh=1.5$  and  $kl=12.0$ , and  $\gamma=10^\circ$  and  $\theta_i=45^\circ$ .

duced because of the increased correlation length. Once again the SSA(2) underpredicts scattering in the back direction, and the third- and fourth-order results show successive improvement. In addition, while not visible in Fig. 3, at very low forward grazing angles ( $<5^\circ$ ) all three orders of the SSA overpredict the scattering strength by slightly more than 1 dB. This behavior is discussed in Sec. II G.

The examples presented in Figs. 2 and 3 illustrate a couple of general points. First, except when the rms slope angle becomes large ( $\gamma > 30^\circ$ ), extending the cross-section series to higher orders increases the region of accuracy to scattering angles further from the specular direction. Second, even the SSA(2) is accurate in the forward-scattering region for modest rms surface slopes except at grazing angles below  $5^\circ$ . (Initial numerical results show that this underprediction of scattering levels in the back direction for smooth surfaces with a Gaussian spectrum does not extend to surfaces with power-law roughness spectra since these surfaces usually contain sufficient small-scale roughness to be rough on the scale of a wavelength. These results will be presented in a future paper.)

## B. Comparison with perturbation theory

The series for the scattering cross section obtained from perturbation theory is in even orders of  $kh$ , beginning at  $(kh)^2$ . Therefore, the lowest-order perturbation cross section is second order in  $kh$  (commonly referred to as the “first-order” perturbation result since the scattered field is found to first order in  $kh$ ) and the next order is fourth order in  $kh$ . By construction, the SSA(2) cross section must reduce to that of lowest-order perturbation theory [PT(2)] in the limit as  $kh$  becomes small. [Note that reference to orders of the SSA is to orders in surface slope; whereas for perturbation theory orders refer to orders in  $kh$ . The PT(2) cross section is of order  $(kh)^2$ .] In Fig. 4 we examine a case when PT(2) is accurate and where the Kirchhoff approximation does not apply. The surface roughness parameters  $kh$  and  $kl$  are 0.1 and 1.4, respectively, the incident angle  $\theta_i$  is  $45^\circ$ , and the

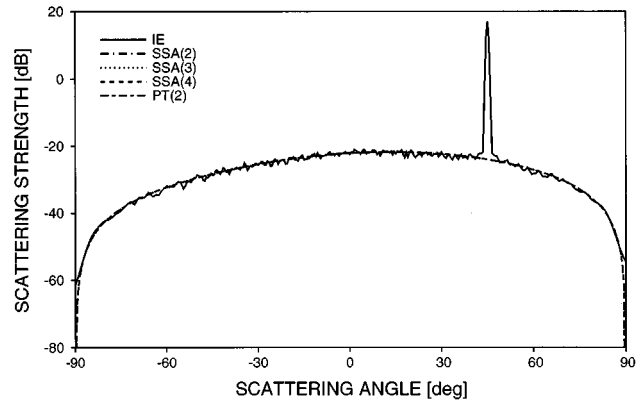


FIG. 4. Comparison of the SSA(2), SSA(3), SSA(4), lowest-order perturbation theory [PT(2)], and IE scattering strengths for a case when PT(2) is accurate. The SSA and PT(2) results are coincident. Here  $kh=0.1$ ,  $kl=1.4$ ,  $\gamma=5.8^\circ$ , and  $\theta_i=45^\circ$ .

rms slope angle  $\gamma$  is  $5.8^\circ$ . For this case, we see that the SSA results for the first three orders are the same as the PT(2) result.

A large number of cases were examined to determine the accuracy of the SSA(2) cross section. The accuracy of the SSA(2) results generally extends beyond the region when PT(2) is accurate, but as with perturbation theory, degradation occurs as the correlation length is increased. There is an important difference between the manners in which PT(2) and the SSA(2) become inaccurate for increasing  $kh$ . In the region of  $kh$ - $kl$  parameter space with moderate slopes ( $\gamma$  less than  $\sim 20^\circ$ ), the SSA(2) remains accurate near the specular direction for all  $kh$ . In contrast, PT(2) becomes inaccurate over the entire angular range for  $kh > 1$ .

We have examined a number of different cases outside the region of validity of PT(2) for which fourth-order PT [PT(4)=PT(2)+ $\sigma_{PT}^{22}$ + $\sigma_{PT}^{13}$ ] is accurate. For the case shown in Fig. 5 with  $kh=0.67$ ,  $kl=2.83$ ,  $\theta_i=45^\circ$ , and  $\gamma=18.4^\circ$ , the SSA(4) cross section is accurate over all scattering angles. In fact, it is more accurate than the PT(4) result which barely meets the  $\pm 1$ -dB criterion for accuracy over a broad range of angles.

Finally, we have examined several cases beyond the region of validity of PT(4), where both PT(4) and the Kirchhoff approximation have limited applicability. For example, in Fig. 6  $kh=1$ ,  $kl=4.3$ , and  $\gamma=18.2^\circ$ . Since  $kh=1$ , perturbation theory is not expected to do well; in fact, the dropout in the PT(4) curve occurs because the cross section becomes negative. The Kirchhoff approximation is better, but for this case, the SSA(4) is clearly the best. It is accurate over almost the entire range of scattering angles.

## C. Comparison with the Kirchhoff approximation

The Kirchhoff approximation (KA) is accurate away from low grazing angles for rough surfaces smooth on the scale of a wavelength, assuming small surface slopes. For a Gaussian roughness spectrum, the KA is accurate over a broad range of scattering angles when  $kl > 6$ , that is when  $l/\lambda > 1$  (Thorsos, 1988). In this section we consider the SSA and KA for several examples with  $kl > 6$ .

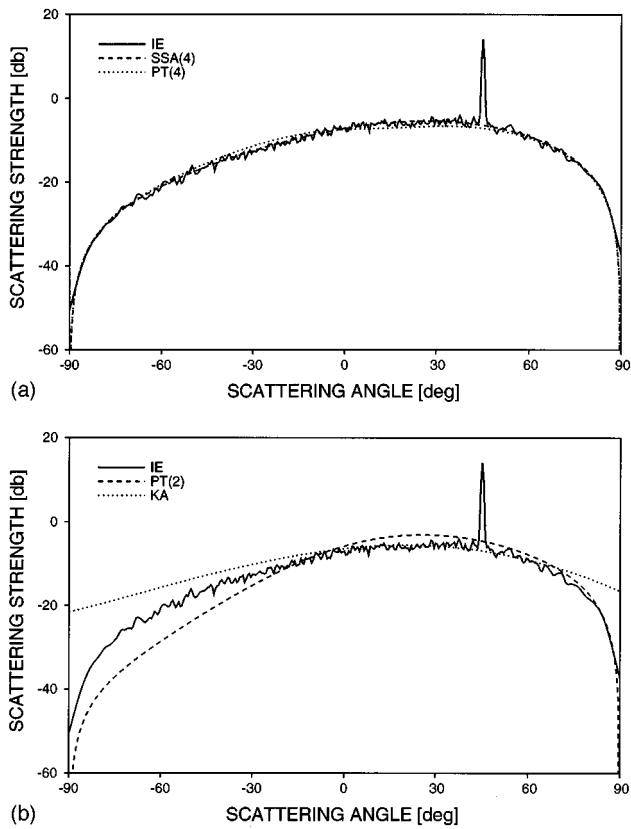


FIG. 5. Comparison of the (a) SSA(4) and fourth-order perturbation theory [PT(4)] and (b) PT(2) and KA scattering strengths with the IE results for a case when neither PT(2) nor the KA is accurate. Here  $kh=0.67$ ,  $kl=2.83$ ,  $\gamma=18.5^\circ$ , and  $\theta_i=45^\circ$ .

In Fig. 3 ( $kh=1.5$ ,  $kl=12$ ,  $\theta_i=45^\circ$ , and  $\gamma=10^\circ$ ) the KA is accurate away from low grazing angles, while perturbation theory does not apply. The SSA(2) result reduces to the KA result in the specular region; the third- and fourth-order results do as well. In the backscatter region the KA is more accurate than the SSA. On the other hand, the KA overpredicts the scattering strength in the forward direction at low grazing angles. In contrast, the SSA scattering strength, even for the lowest order, is remarkably good in this same region, although as explained later the SSA results

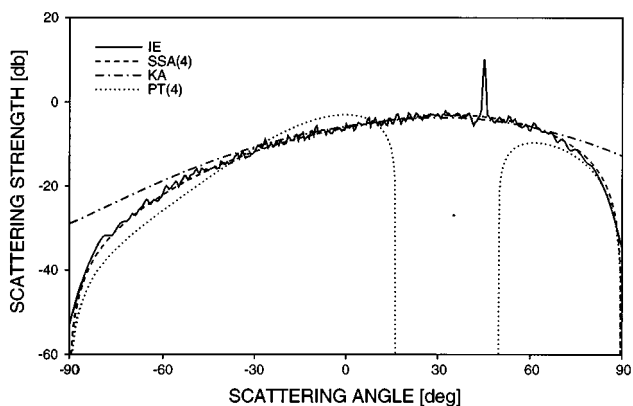


FIG. 6. Comparison of the SSA(4), KA, and PT(4) scattering strengths with the IE results for a case when neither PT(4) nor the KA is accurate. Here  $kh=1.0$ ,  $kl=4.3$ ,  $\gamma=18.2^\circ$ , and  $\theta_i=45^\circ$ .

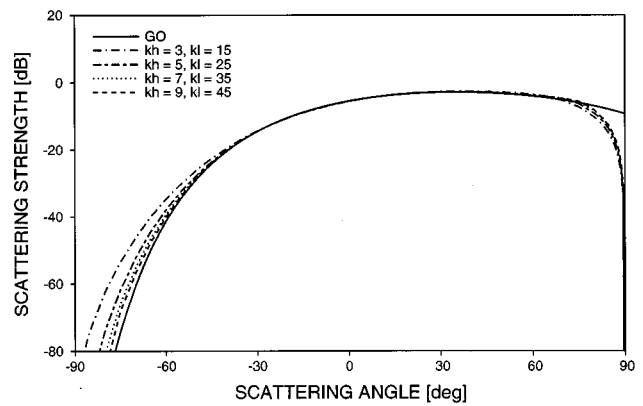


FIG. 7. Reduction of the SSA(4) result to the geometrical optics result (GO) as  $kh$  and  $kl$  are increased for a fixed rms slope angle  $\gamma=15.8^\circ$  and an incident angle of  $45^\circ$ . The SSA(4) scattering strength reduces analytically to the GO result in the high-frequency limit, but the reduction is nonuniform in scattering angle and, at low grazing angles, is very slow.

are somewhat high at the lowest forward grazing angles.

The SSA(4) cross section reduces to the KA cross section as the frequency is increased (Voronovich, 1985; Thorsos and Broschat, 1995), which suggests that the SSA may become significantly inaccurate at low grazing angles for high frequencies. To study the reduction of the SSA(4) to the KA, we considered several cases with fixed surface slope angle and increased the frequency, that is, we increased both  $kh$  and  $kl$  so that the surface slope angle remained constant. We then compared the SSA and KA results and found that the reduction occurs quickly in the specular region and much more slowly away from this region, especially near grazing. In fact, as will be seen shortly, the SSA remains quite good at low grazing angles as the frequency is increased.

In the high-frequency limit ( $k \rightarrow \infty$ ) both the SSA(4) and KA cross sections reduce to the geometrical optics (GO) expression

$$\sigma_{GO}(\theta_s, \theta_i) = \frac{(1 + \cos \theta_i \cos \theta_s - \sin \theta_i \sin \theta_s)^2}{(\cos \theta_i + \cos \theta_s)^3} \times \exp\left\{-\frac{(\sin \theta_i - \sin \theta_s)^2 l^2}{4(\cos \theta_i + \cos \theta_s)^2 h^2}\right\}.$$

In Fig. 7, we show a case for  $l/h=5$ , an rms slope angle  $\gamma$  of  $15.8^\circ$ , and an angle of incidence  $\theta_i$  of  $45^\circ$ . As we increase both  $kh$  and  $kl$ , the SSA(4) scattering strength approaches the GO result. This reduction is nonuniform in scattering angle: Over a large range of scattering angles reduction occurs quickly; however, at grazing angles less than about  $10^\circ$  the reduction is quite slow. In the backscatter region, the SSA(4) curves lie close to the KA curves (not shown) for each case, except for  $\theta_s < -80^\circ$  as in Fig. 3, as both converge to the GO limit. In contrast, for  $\theta_s > 70^\circ$ , the KA scattering strengths all reduce to the GO limit, while the SSA(4) results converge very slowly to this limit. In Fig. 8 we compare the SSA(4) prediction with the GO and shadowed GO results (Wagner, 1967) in the forward-scattering region for the highest-frequency case in Fig. 7. We also show the integral equation scattering strength. The two GO approximations differ significantly only for scattering angles greater

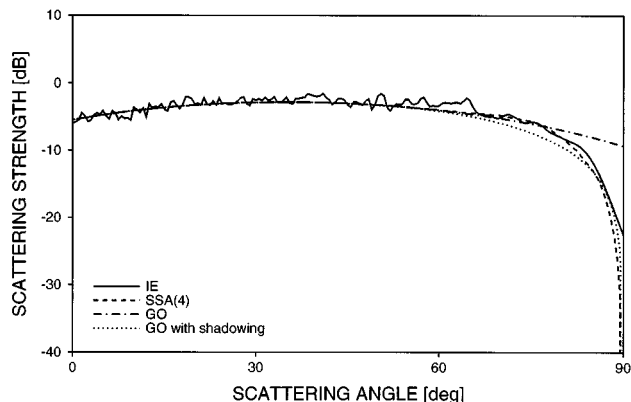


FIG. 8. Comparison of the SSA(4), GO, GO with shadowing, and IE scattering strengths for  $kh=9$ ,  $kl=45$ ,  $\gamma=15.8^\circ$ , and  $\theta_i=45^\circ$ . Note that the SSA(4) result is more accurate in the forward-scattering region than the shadowed geometrical optics result.

than approximately  $70^\circ$ . We see in Fig. 8 that the SSA(4) is quite good in this region; in fact, it is superior to both the unshadowed and shadowed GO approximations. Even the SSA(2) cross section gives results superior to those of the Kirchhoff or GO approximations, while it is as readily calculated as the KA cross section.

To explore the relationship between the surface slope and the accuracy of the SSA, we focus on the effects of changing  $kh$  for a fixed  $kl$  and  $kl$  for a fixed  $kh$ , that is, increasing and decreasing the rms surface slope, respectively, in Secs. II D and II E. Then in Sec. II F we consider angles of incidence other than  $45^\circ$ . Finally, in Sec. II G we return to the behavior of the SSA at low forward grazing angles when the correlation length is increased.

#### D. Increasing the rms surface height for a fixed correlation length

The SSA is not restricted to small surface roughness and, as shown previously, can be accurate over a broad range of scattering angles for moderate surface slopes. As explained in Sec. I, the terms of the  $T$ -matrix series depend on more than just simple surface slope. However, we might still expect a relationship between the accuracy of the SSA and rms surface slope values. In fact, when we increase the rms slope for a fixed correlation length by increasing the rms surface height, the SSA(4) results become visibly high in the forward-scattering direction. In Fig. 9(a) and (b) we have chosen  $kl$  to be 2.83 and have used a  $kh$  of 1.33 and 2.0, respectively. Figures 5, 9(a), and 9(b) correspond to increasing rms slope angles from  $18.5^\circ$  to  $45^\circ$  for a fixed  $kl$ . The incident angle is  $45^\circ$ . When  $kh=1.33$  and  $\gamma=33.7^\circ$  [Fig. 9(a)], the accuracy of the SSA(4) scattering strength starts to degrade at low forward grazing angles where the result is too high (the error extends up to about 1.5 dB). This overprediction becomes more pronounced and occurs at higher grazing angles as the rms slope is further increased as shown in Fig. 9(b). In addition, as the rms slope angle is increased up to and beyond  $45^\circ$ , scattering levels become high at low backscatter grazing angles as well. This overprediction, just becoming evident in Fig. 9(b), also becomes greater and occurs at higher grazing angles as the rms slope is further increased.

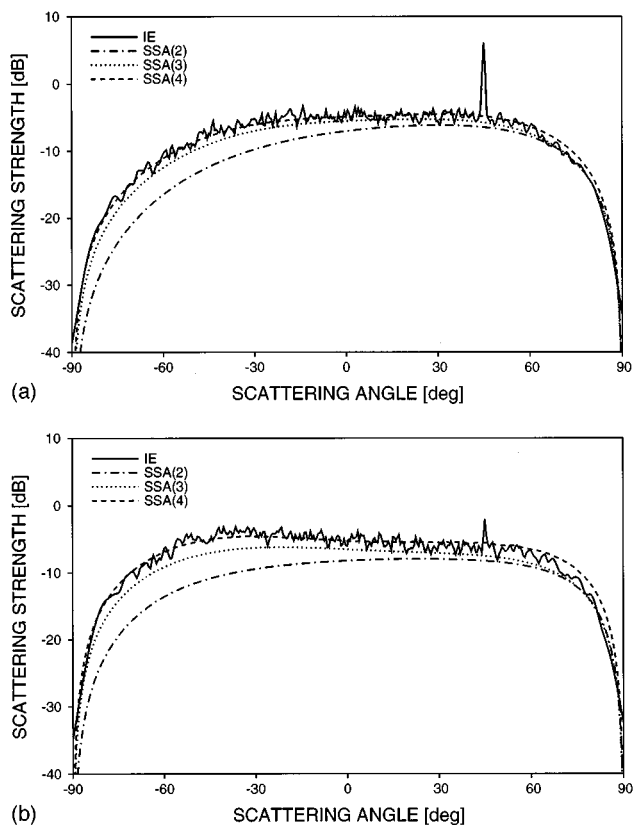


FIG. 9. The effect of increasing the slope by changing  $kh$  for a fixed  $kl$  and fixed incident angle, where  $kl=2.83$  and  $\theta_i=45^\circ$ , (a)  $kh=1.33$ ,  $\gamma=33.6^\circ$ , and (b)  $kh=2.0$ ,  $\gamma=45.0^\circ$ . Also, compare the result in Fig. 5 ( $kh=0.67$ ,  $\gamma=18.5^\circ$ ). As the rms slope is increased beyond  $30^\circ$ , the SSA(4) scattering strength becomes high in the forward direction. When it is increased beyond  $45^\circ$ , the SSA(4) scattering strength becomes high in the low back direction as well.

A similar study was done for a fixed  $kl$  of 12.0 and an incident angle of  $45^\circ$ ; the results show the SSA(4) scattering strength becomes inaccurate at a smaller rms surface slope for this higher-frequency case.

One way of observing the decrease in accuracy of the SSA with increasing slope is to compare the third- and fourth-order results. When  $\sigma^{(2)}$ ,  $\sigma^{(3)}$ , and  $\sigma^{(4)}$  are coincident as in Fig. 4 the terms  $\sigma_{01}$  and  $\sigma_{11}$  make negligible contributions to the cross section, and the first three orders of the SSA are all found to be accurate. When the difference between  $\sigma^{(3)}$  and  $\sigma^{(4)}$  is small,  $\sigma_{11}$  makes a negligible contribution to the scattering strength and the third- and fourth-order results are found to be accurate. When the difference between  $\sigma^{(3)}$  and  $\sigma^{(4)}$  becomes significant, the fourth-order result may no longer be accurate. To determine how large this difference must be, we examined  $\Delta SS = 10 \log_{10}[\sigma^{(4)}/\sigma^{(3)}]$  for the cases given in Figs. 5 and 9 as well as for other cases. We found that for a fixed  $kl$  and increasing  $kh$ , that is, for increasing slopes,  $\Delta SS$  shows the largest increase near grazing in both the forward- and backward-scattering directions. This is consistent with our discussion in the preceding paragraph. Furthermore, larger values of  $kl$  have larger values of  $\Delta SS$  in the backward-scattering direction relative to the forward-scattering direction for the same values of slope. Unfortunately, the relation-

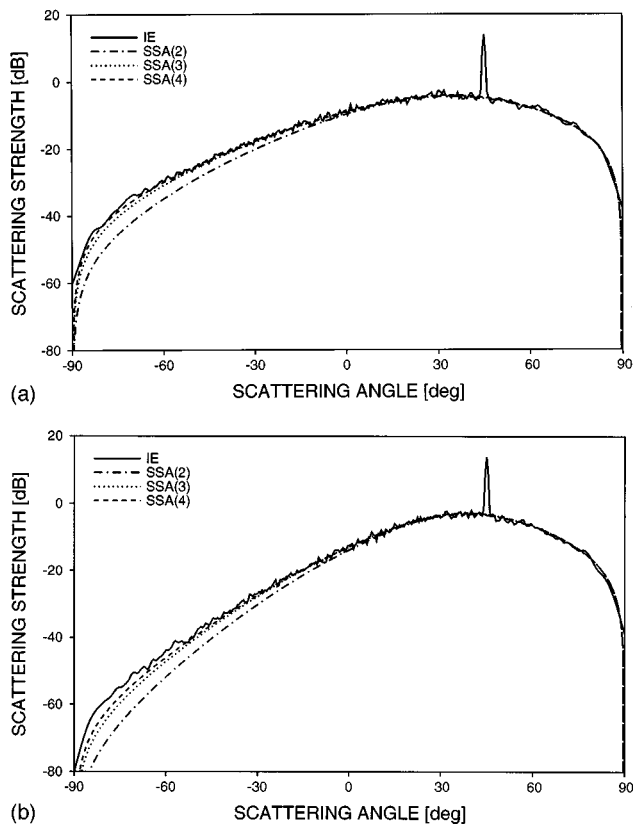


FIG. 10. The effect of decreasing the slope by changing  $kl$  for a fixed  $kh$  and fixed incident angle, where  $kh=0.67$  and  $\theta_i=45^\circ$ , (a)  $kl=4.24$ ,  $\gamma=12.6^\circ$ , and (b)  $kl=6.28$ ,  $\gamma=8.6^\circ$ . Also, compare the result in Fig. 5 ( $kl=2.83$ ,  $\gamma=18.5^\circ$ ). As the correlation length is increased beyond about 5, the SSA(4) scattering strength becomes somewhat low in the back direction.

ship between  $\Delta SS$  and the accuracy of  $\sigma^{(4)}$  cannot be quantified in a simple manner.

### E. Increasing the correlation length for a fixed rms surface height

Next it is of interest to examine what occurs as the correlation length is increased for a fixed rms surface height. This is equivalent to decreasing the rms slope for a fixed  $kh$ . In Fig. 10(a) and (b) we have chosen  $kh$  to be 0.67 and have used a  $kl$  of 4.24 and 6.28, respectively. Figures 5, 10(a), and 10(b) correspond to decreasing rms slope angles from  $18.5^\circ$  to  $8.6^\circ$  for a fixed  $kh$ . The incident angle is  $45^\circ$ . For  $kl$  up to 4.24, there is excellent agreement between the SSA(4) and exact results. However, beginning at a  $kl$  of about 5 the SSA(4) underpredicts scattering in the back direction. This underprediction is true in Fig. 3 as well, where  $kh=1.5$  and  $kl=12$ . An additional study was done for a fixed  $kh$  of 2.0, an incident angle of  $45^\circ$ , and  $kl$  varying between 4 and 15 (equivalent to rms slope angles between  $35.3^\circ$  and  $10.7^\circ$ ) with similar results, that is, as the correlation length is increased, backscatter is underpredicted. The discrepancy between the SSA and exact results is greater at smaller backward grazing angles and worsens as the correla-

tion length is increased. In the forward direction the results become slightly high at forward grazing angles smaller than  $5^\circ$  as  $kl$  is increased.

Again we examined  $\Delta SS=10 \log_{10}[\sigma^{(4)}/\sigma^{(3)}]$ , this time for the cases shown in Figs. 5 and 10 as well as for other cases. We found that for a fixed  $kh$  and increasing  $kl$ , that is, for decreasing slopes,  $\Delta SS$  becomes larger in the backward-scattering direction, indicating the decrease in accuracy of the fourth-order result and reflecting the importance of the  $\sigma_{11}$  term in the back direction.

The underprediction of backscatter by the SSA for large  $kl$  and small  $kh$  can be explained as follows: The SSA  $T$  matrix is expanded in powers of the surface profile (or its Fourier transform) and the resulting terms are equated with those of the standard perturbation series  $T$  matrix (Thorsos and Broschat, 1995). To find  $T_0$ , terms up to first order in the surface profile are retained; to find  $T_1$ , terms up to second order are retained; and to find  $T_2$ , terms up to third order are retained. In earlier work (Thorsos and Jackson, 1989) it was shown that for a Gaussian roughness spectrum, lowest-order perturbation theory becomes inaccurate as the correlation length is increased even when  $kh \ll 1$ . In particular, the perturbation prediction for scattering in the back direction becomes low. However, in the forward direction the results are quite accurate, even for very large  $kl$ . When the perturbation cross section is computed to fourth order in  $kh$ , scattering levels in the back direction are accurately predicted for larger  $kl$ . For the SSA the same behavior occurs for small  $kh$  since the SSA reduces to PT in this region, but interestingly enough, it occurs for larger  $kh$  as well. For general  $kh$  the SSA(2) result underpredicts scattering in the back direction as the correlation length is increased. The results improve when the third- and fourth-order cross sections are used, particularly at fourth order which includes two factors of  $T_1$ . Thus, if the SSA were extended to include the  $T_2$  term, we would expect our results to improve even further in the back direction for large correlation lengths.

### F. Other angles of incidence

In the previous sections we considered examples with incident angles of  $45^\circ$ . In this section we briefly discuss other angles of incidence and present a few examples. For the cases studied, we noted that when the scattering strength results are accurate over all angles of scatter for an incident angle of  $45^\circ$ , in general they are good for incident angles up to  $80^\circ$ . When the results are low in the backscatter region for an incident angle of  $45^\circ$ , they are better for  $0^\circ$  incidence and worse for  $80^\circ$  incidence. These results are illustrated in Figs. 11 and 12. In Fig. 11(a) and (b) the incident angles are  $0^\circ$  and  $80^\circ$ , respectively, for the same roughness parameters used in Fig. 5,  $kh=0.67$ ,  $kl=2.83$ , and  $\gamma=18.5^\circ$ . In Fig. 11(b), and later in Fig. 12(b), the coherent component has been subtracted from the integral equation result (see Thorsos, 1990, for details) so the specular peak, which is wider at lower grazing angles, does not obscure the incoherent component. For the results presented in Fig. 11(a) and (b) the SSA(4) scattering strengths show excellent agreement with the integral equation results over the entire range of scattering angles. However, when the correlation length is in-

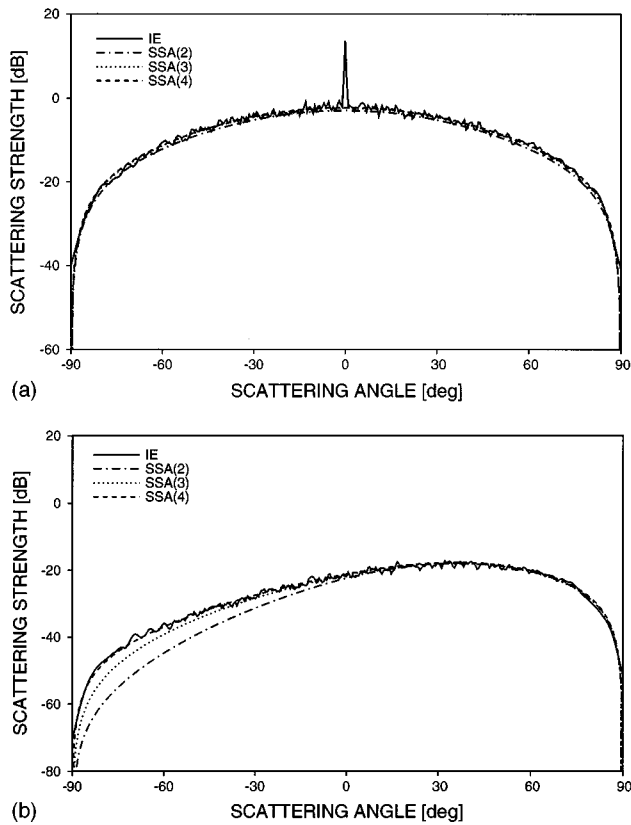


FIG. 11. Comparison of the SSA(2), SSA(3), SSA(4), and IE scattering strengths for the case shown in Fig. 5 but with an incident angle of (a) 0° and (b) 80°. In (b) the coherent component has been subtracted from the IE result to facilitate comparisons of the incoherent scatter.

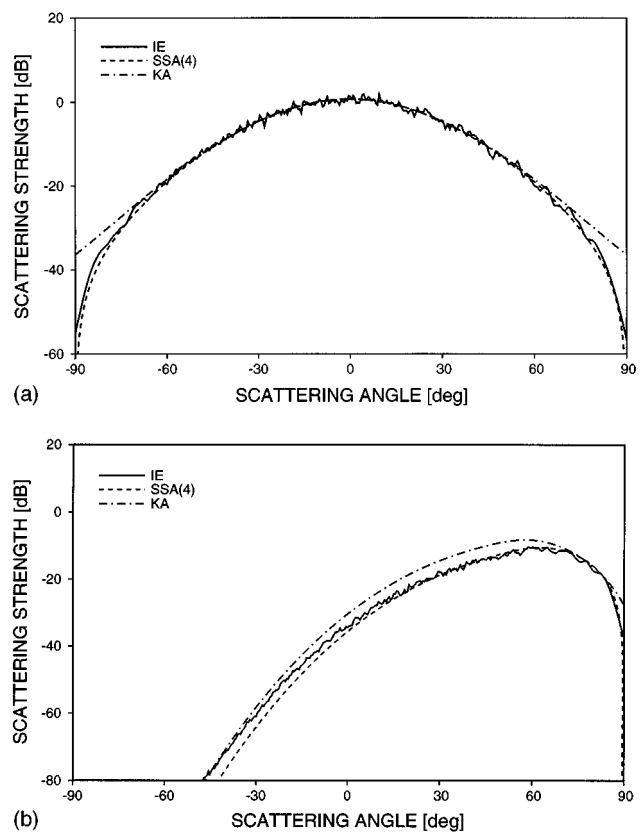


FIG. 12. Comparison of the SSA(4), KA, and IE scattering strengths for the case shown in Fig. 3 but with an incident angle of (a) 0° and (b) 80°. In (b) the coherent component has been subtracted from the IE result to facilitate comparisons of the incoherent scatter.

creased, the accuracy of the SSA is not as good. For example, in Fig. 12(a) and (b) we consider incident angles of 0° and 80° for the same surface parameters used in Fig. 3,  $kh = 1.5$ ,  $kl = 12$ , and  $\gamma = 10^\circ$ . For the 0° case, the SSA(4) clearly performs better than the KA at low scattered grazing angles. Also, for the 0° incidence case the SSA is accurate over a larger range of scattering angles than for the 45° incidence case shown in Fig. 3. For the 80° case, the decrease in accuracy of the SSA is evident in comparison to Fig. 3, but still the result is better than that of the KA.

### G. Behavior at low forward grazing angles

As mentioned several times in earlier sections, the SSA scattering strength can become somewhat high at low forward grazing angles as the correlation length is increased. However, because this occurs when the curves are sloping steeply downward, it is difficult to detect the difference between them in the plots presented thus far. The region of inaccuracy occurs at very small grazing angles, and the angular resolution of the exact results decreases with grazing angle, which also obscures the difference. To highlight the difference between the integral equation and SSA(4) results, in Fig. 13 we show part of the forward grazing angle region for the case shown in Fig. 3. In addition, to reduce the effects of fluctuations the integral equation result shown is the average of nine different runs, each using 50 surface realizations. Error bars provide an estimate for the uncertainty in the Monte Carlo result for the scattering strength based on all 450 surfaces. The SSA(4) result becomes high at very low forward grazing angles, exceeding 1 dB at approximately 87°.

the Monte Carlo result for the scattering strength based on all 450 surfaces. This estimate is obtained by dividing the standard deviation of the nine 50-surface averages by the square root of nine. In this example, the SSA(4) overpredicts the forward-scattering strength by 1–1.5 dB in this very low grazing region. The crossover, which occurs at about 88.6° in Fig. 13 with the integral equation curve rising above the

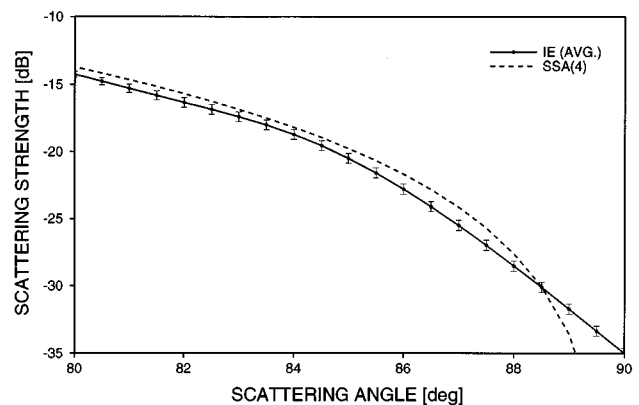


FIG. 13. The forward grazing region for the case shown in Fig. 3. The IE result is the average of nine different runs, each using 50 surface realizations. Error bars provide an estimate for the uncertainty in the Monte Carlo result for the scattering strength based on all 450 surfaces. This estimate is obtained by dividing the standard deviation of the nine 50-surface averages by the square root of nine. The SSA(4) result becomes high at very low forward grazing angles, exceeding 1 dB at approximately 87°.

SSA(4) curve as  $90^\circ$  is approached, is due in part (and perhaps entirely) to the reduced angular resolution of the integral equation result near  $90^\circ$ . Stated another way, the integral equation result is found with surfaces of finite length, while the SSA(4) curve is for infinite length surfaces. Scattering strengths for these two types of surfaces differ significantly only within a few degrees of grazing, with the finite surface lengths yielding higher scattering strengths in this region. Thus, it is consistent with our results for the SSA(4) to have a positive error all the way to a scattering angle of  $90^\circ$  ( $0^\circ$  grazing). While the finite angular resolution of the integral equation result affects the comparison with the SSA(4) at very low grazing angles, studies with longer surface lengths which give improved angular resolution indicate that our comparison correctly shows the scattering angle at which the error first exceeds 1 dB as  $90^\circ$  is approached. We have examined this behavior for a large number of cases and find a 1–2 dB overprediction at very low grazing angles to be typical of the SSA(4).

We find that the behavior of the low grazing angle error depends on both the correlation length and the rms slope. In the region when perturbation theory is accurate, the error does not occur. As the correlation length is increased, the inaccuracy occurs earlier for steeper slopes. Furthermore, the inaccuracy begins at higher grazing angles for steeper slopes. For example, for a slope angle of  $25^\circ$ , the inaccuracy begins at a scattering angle of about  $85.5^\circ$ ; whereas for a slope angle of  $15^\circ$  it begins at about  $87^\circ$ . We suspect that this low grazing angle error is caused by nonlocal multiple scattering that is not adequately treated by the SSA.

### III. SUMMARY

Expressions for the second-, third-, and fourth-order small slope bistatic scattering cross sections have been presented together with extensive numerical results for scalar wave scattering from 1-D surfaces with Gaussian statistics and a Gaussian roughness spectrum. These results were compared with exact numerical results as well as with the results of other approximate techniques.

The initial appeal of the SSA was its formulation as a systematic series, its reduction to perturbation theory which is inherent in the derivation, and its reduction to the Kirchhoff approximation under appropriate conditions when the  $T$  matrix is found to second order in slope. Also, the theory is manifestly reciprocal at each order and, at low orders, the formally averaged expressions for the scattering cross section are numerically tractable. In this numerical study we have shown that the appeal of the SSA extends further. The fourth-order SSA cross section is remarkably accurate for surfaces with rms slope angles up to about  $30^\circ$ . Even with an rms surface slope angle of  $45^\circ$ , the fourth-order result is accurate over a wide range of scattering angles. As the surface correlation length is increased, the SSA results become low in the back direction and slightly high at forward grazing angles less than  $5^\circ$ . Finally, although the fourth-order SSA

cross section analytically reduces to the geometrical optics result in the high-frequency limit, we found in our numerical studies that the reduction is nonuniform in the scattering angle and, at low forward grazing angles, occurs very slowly. Comparison with exact results shows that the SSA gives better results than geometrical optics with shadowing in this region.

Because the SSA reduces to low-order perturbation theory when the latter is accurate and to the Kirchhoff approximation in the specular region, we expect it might be good for multiscale surfaces. In fact, preliminary results show that for a Pierson–Moskowitz spectrum the SSA gives accurate results even in the back direction (Broschat and Thorsos, 1995). This is the subject of further study.

### ACKNOWLEDGMENTS

This work was supported by the Office of Naval Research, Code 3210A. The authors wish to acknowledge helpful comments made by the reviewers.

- Berman, D. H. (1991). "Simulations of rough interface scattering," *J. Acoust. Soc. Am.* **89**, 623–636. Appendix A in this reference shows that  $\langle T(k_{sx}, k_{ix}) \rangle$  vanishes unless  $k_{sx} = k_{ix}$  and that  $\langle T(k_{sx}, k_{ix}) T(k'_{sx}, k'_{ix})^* \rangle$  vanishes unless  $(k_{ix} = k'_{ix})$ . It does not show that  $\langle T(k_{sx}, k_{ix}) \rangle$  and  $\langle T(k_{sx}, k_{ix}) T(k'_{sx}, k'_{ix})^* \rangle$  must be proportional to  $\delta(k_{sx} - k_{ix})$  and  $\delta(k_{ix} - k'_{ix})$ , respectively, since other distributions were not ruled out; these properties are needed to obtain (3). An extension of the arguments given in Berman's Appendix A can be used to show these moments of  $T$  must be proportional to delta functions, but the analysis is not presented here.
- Broschat, S. L. (1993). "The small slope approximation reflection coefficient for scattering from a 'Pierson-Moskowitz' sea surface," *IEEE Trans. Geosci. Remote Sens.* **31**, 1112–1114
- Broschat, S. L., and Thorsos, E. I. (1995). "Numerical studies of the small slope approximation for rough surface scattering using a Pierson–Moskowitz spectrum," *J. Acoust. Soc. Am.* **97**, 3404.
- Ishimaru, A. (1978). *Wave Propagation and Scattering in Random Media* (Academic, New York), Vol. II, Chap. 21.
- Parzen, E. (1962). *Stochastic Processes* (Holden-Day, San Francisco), pp. 88–97.
- Thorsos, E. I. (1988). "The validity of the Kirchhoff approximation for rough surface scattering using a Gaussian roughness spectrum," *J. Acoust. Soc. Am.* **83**, 78–92.
- Thorsos, E. I. (1990). "Acoustic scattering from a 'Pierson–Moskowitz' sea surface," *J. Acoust. Soc. Am.* **88**, 335–349.
- Thorsos, E. I., and Broschat, S. L. (1995). "An investigation of the small slope approximation for scattering from rough surfaces. Part I. Theory," *J. Acoust. Soc. Am.* **97**, 2082–2093.
- Thorsos, E. I., and Jackson, D. R. (1989). "The validity of the perturbation approximation for rough surface scattering using a Gaussian roughness spectrum," *J. Acoust. Soc. Am.* **86**, 261–277.
- Voronovich, A. G. (1985). "Small-slope approximation in wave scattering by rough surfaces," *Sov. Phys. JETP* **62**, 65–70.
- Voronovich, A. G. (1986). "A unified description of wave scattering at boundaries with large and small scale roughness," *Progress in Underwater Acoustics*, edited by Harold M. Merklinger (Plenum, New York).
- Wagner, R. J. (1967). "Shadowing of randomly rough surfaces," *J. Acoust. Soc. Am.* **41**, 138–147.
- Yang, T. Q., and Broschat, S. L. (1992). "A comparison of scattering model results for two-dimensional randomly rough surfaces," *IEEE Trans. Antennas Propag.* **40**, 1505–1512.
- Yang, T. Q., and Broschat, S. L. (1994). "Acoustic scattering from a fluid–solid interface using the small slope approximation," *J. Acoust. Soc. Am.* **96**, 1796–1804.